femington

Int. J. Adapt. Manag. Bus. Intell. (2026) 1(2):1–15
Article ID: IJAMBI-2026-648

Spatially-Anchored Small Multiples for Enhanced Geographic Data Exploration

Vadada Venkata Naga Dinesh
venkatanagadineshvadada@gmail.com
Independent Researcher

Abstract

This paper investigates the application of spatially anchored small multiples, commonly referred to as geofaceting, for the analysis and visualization of complex demographic data. This study shows how arranging individual panels according to the approximate geographical locations of corresponding regions facilitates the preservation of spatial proximity relationships while enabling the exploration of high-dimensional within-region patterns using the geofacet R package. A case study illustrates the use of geofaceted layouts and modern visualizations, such as Lexis surfaces and ternary shades, based on mortality data of young Mexican adults across states. Temporal, demographic, and regional variations can now be portrayed together whilst remaining interpretable and visually coherent. The paper also implements a controlled investigation of cognitive efficiency to compare geofaceted arrangements with standard alphabetical panel arrangements. The findings indicate that spatial organization and improved within-panel visual encoding can provide benefits. Geofaceting offers a suitable framework for visualization practitioners looking to integrate complex multivariable information with a meaningful geographic context.

Keywords

• Geovisualization • Small Multiples • Geofaceting • Spatial Data Visualization • Lexis Surfaces • Ternary Color Coding • Mortality Analysis • Mexico

1. Introduction

1.1 The Challenge of Multi-Dimensional Spatial Visualization

Geographic data visualization must simultaneously convey quantitative values and spatial context: the analyst needs to know not only what the numbers are, but where they occur and how neighboring regions relate to one another [1]. This dual requirement grows harder as the dimensionality of the underlying data expands beyond simple univariate measures. Traditional choropleth maps handle this well for a single variable, encoding values through color intensity across dozens or hundreds of regions. The approach collapses, however, once an analyst needs to represent multiple dimensions at once time series, multivariate compositions, age-specific rates, or cause-specific contributions each of which exceeds the single channel of color intensity. [2]

Several strategies address this challenge, each with limitations. Small multiples, popularized by Tufte [3], present a separate chart per region in a regular grid, accommodating rich within-panel content but destroying geographic relationships adjacent grid panels rarely correspond to neighboring regions, forcing the analyst to consult an external map. Animation sequences leverage temporal integration but prevent

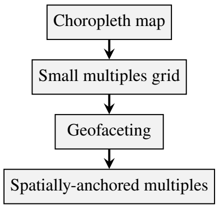

Figure 1: Evolution of spatial visualization approaches. Each generation adds capacity for additional data dimensions while preserving geographic interpretability.

simultaneous comparison across periods; overlaying series on a single map creates clutter; and interactive pan/hover systems shift cognitive burden from interpretation to navigation.

Geofaceting resolves this tension by arranging small multiples according to the approximate geographic position of their corresponding regions north at top, south at bottom, and so on so the composite image functions simultaneously as a set of detailed charts and a schematic map. This delivers three benefits: (1) region identification becomes immediate, without consulting external references; (2) spatial patterns emerge directly from clusters of visually similar panels; and (3) the arrangement preserves the analyst's mental map of the territory [1], enabling rapid alternation between detailed inspection and holistic assessment.

The core insight has been independently rediscovered many times: Galton's 1863 meteorographica charts arranged European weather stations in an approximate geographic grid, and nineteenth-century French cartographers (e.g., Minard) overlaid small plots directly on base maps. What distinguishes contemporary geofaceting is the complete separation of small multiples from any underlying base map, trusting panel arrangement alone to convey geographic context and maximizing space available for data display.

1.2 Contribution and Scope

This paper makes four contributions building on existing geofaceting methods and the small-multiples literature. First, we articulate a design framework for geofaceted Lexis surfaces and compositional cause-of-death data, identifying tradeoffs that arise when combining spatial anchoring with age-period representations. Second, we provide a substantive application young adult mortality across Mexican states, 1990 to 2015 showing that geofaceting reveals spatial patterns invisible in alphabetical layouts. Third, we integrate geofaceting with ternary color coding for three-part compositional data, an extension not previously implemented in spatially-anchored small multiples. Fourth, we report a controlled experiment quantifying the cognitive-efficiency gains of geofaceted versus alphabetical layouts, providing empirical evidence for a benefit long assumed but rarely tested.

The remainder proceeds as follows. Section 3 describes data, demographic methods, and the Mexican geofacet grid. Section 4 presents geofaceted mortality visualizations. Section 5 details ternary color coding for compositional cause-of-death data. Section 6 reports the cognitive-efficiency experiment. Section 7 discusses limitations and generalizability, and Section 8 concludes.

2. Related Work

Geofaceting sits at the intersection of five literatures: the cognitive foundations of small multiples, cartographic visualization, demographic visualization, ternary composition methods, and grid-layout algorithms. We focus on three questions that directly informed our design: (1) what perceptual mechanisms make spatial arrangement more efficient than alphabetical ordering; (2) how have prior demographic visualizations compared regions, and what gaps remain; and (3) what prior spatially-arranged small multiples exist, and how does integration with ternary color coding extend.

2.1 Cognitive foundations and cartographic context

Tufte's account of small multiples [3] established that grid arrangement exploits parallel visual processing for comparison; Bertin's semiology of graphics [2] showed that spatial arrangement itself carries meaning, though his matrices ordered regions alphabetically or by value rather than spatially. Cleveland and McGill [4] demonstrated that position along a common scale is the most accurately perceived visual channel, a finding later confirmed at scale by Heer and Bostock [5]; geofaceting exploits exactly this channel by encoding geography through panel position. Ware's comprehensive treatment of visual perception for design [1] further establishes that spatial position is processed pre-attentively, making it one of the most efficient channels for encoding categorical and ordinal information. Tobler's first law of geography that near things are more related than distant things [6] motivates placing neighboring regions in adjacent panels so that spatial autocorrelation becomes directly visible.

Contemporary data visualization practice has increasingly emphasised the importance of integrating analytical workflows with intuitive interfaces. Recent work by Parekh [7] on responsive interfaces for end-user service orchestration demonstrates how thoughtful interface design can reduce cognitive load and improve analytical efficiency, principles that extend directly to the design of geofaceted visualisation systems. Similarly, Agarwal [8] has shown how visual pathways to data preparedness can empower AI projects through insightful analytic visualisation, underscoring the value of well-designed visual interfaces for complex data exploration. The integration of spatial anchoring with small multiples represents a natural progression of these interface-design principles into the geographic visualisation domain.

2.2 Demographic visualisation and compositional colour coding

The Lexis surface, developed for age-period mortality analysis and treated comprehensively by Rau and colleagues [9], is our core within-panel technique; that work explicitly notes that alphabetically arranged panels obscure regional comparison, directly motivating our geofaceted extension. Pebesma's `sf` package [10] underlies the geospatial tooling that could eventually automate grid construction from polygon boundaries.

Recent demographic research has leveraged advanced computational methods to address complex population health questions. Tiwari [11] developed a scalable framework for stabilising epidemic surveillance through real-time correction of incomplete public health data, demonstrating the importance of robust demographic estimation procedures that inform visualisation design. Kasireddy [12] advanced scalar-on-function regression approaches for healthcare management applications, illustrating how sophisticated analytical methods can be paired with effective visualisation to support decision-making. Additionally, Idnani [13] explored human capital depreciation and gender-specific wage trends, showing how demographic analysis benefits from clear, comparative visual representations.

For compositional data, Aitchison's log-ratio framework [14] established that simplex-constrained data require specialised visualisation; Wickham's `ggplot2` grammar [15], extended to ternary diagrams by Hamilton and Ferry's `ggtern` [16] and to ternary colour encoding by Schöley and Kashnitsky's `tricolore` [17], provides the technical foundation for our ternary-encoded Lexis surfaces.

2.3 Grid layout and applications

Wilkinson's grammar of graphics [18] suggests geographic coordinates could serve directly as position aesthetics, but direct mapping produces overlapping panels for closely-spaced regions; grid construction resolves this while preserving approximate adjacency.

Recent applications in data science and analytics have explored various aspects of visual data exploration. Raichur [19] developed data-driven approaches for identifying irregular patterns in complex datasets, highlighting the need for flexible visualisation tools that adapt to data characteristics. Amin [20] optimised in-database analytics for dynamic data exploration, emphasising the importance of efficient data retrieval and presentation in analytical workflows. Syed [21] contributed to semantic synthesis of analytical pipelines, demonstrating how automated workflow composition can support predictive data science, including visualisation components. The method of geofaceting can be seen as part of this broader trend toward creating more intuitive and efficient analytical workflows.

Beyond demographic applications, geofaceting principles have found utility across diverse domains. Bachu [22] demonstrated the application of time-series and machine learning techniques for energy demand visualisation, while Chebrolu [23] employed AI-guided approaches for siting EV charging infrastructure in urban transport networks. These applications underscore the versatility of geofaceted approaches for spatial decision support. Bhuekar [24] developed AI-driven supply chain analytics with adaptive decisioning via fuzzy behavioural models, while Sarakam [25] created high-performance real-time data stores for streaming analytics, each demonstrating the importance of effective visualisation in domain-specific applications. Parashar [26] enhanced association rule mining with a cluster-based approach for inventory management, and Parise [27] developed adaptive machine learning frameworks for personalised quality evaluation, both suggesting new directions for geofaceted visualisation in their respective domains. Recent work by Abhishek [28] on transformer-based inference of residential EV charging patterns demonstrates how modern machine learning can inform spatial data visualisation.

Despite this literature, three gaps remain, which this paper addresses: no prior work has experimentally quantified the cognitive-efficiency benefit of spatial versus conventional panel arrangement; existing geofacet applications use comparatively simple within-panel charts rather than Lexis surfaces; and ternary colour encoding has previously been applied to static maps or single panels, not to geofaceted, age-period surfaces. We also contribute an original Mexican-states geofacet grid as a community resource.

3. Data And Methods

3.1 Mexican Mortality Data

Our empirical demonstration draws on detailed mortality records from Mexico spanning 1990 to 2015. Death registration data (cause of death coded to ICD standards) come from the Mexican Statistical Office; population estimates, adjusted for age misstatement, underenumeration, and migration, come from the Mexican Population Council. The dataset covers all 32 Mexican federal entities. We focus on males aged 15 to 49, the demographic segment most affected by the escalation of homicidal violence since 2005 and the group exhibiting the sharpest geographic heterogeneity in mortality profile, making it well suited to demonstrate geofaceted visualisation.

3.2 Demographic Estimation Procedures

We constructed period life tables for each state-year combination, smoothing death rates over age and time with two-dimensional P-splines under penalised likelihood (smoothing parameter chosen via

Table 1: Mexican states by region and geofacet grid position

Region	States	Grid rows	Grid columns
Northwest	6	1-3	1-4
Northeast	4	1-3	5-7
West	5	4-6	1-3
Center	8	4-7	4-6
South	5	7-9	2-5
Southeast	4	8-10	6-8

generalised cross-validation per state-sex combination). Temporary life expectancy between ages 15 and 49 was calculated following Arriaga's method, summarising mortality over the young-adult years without extrapolation to sparse older ages. Such smoothing and estimation procedures are critical for reliable demographic analysis, as emphasised in recent work on real-time data correction [11] and functional regression approaches [12].

3.3 Benchmark Construction and Decomposition

To assess potential for mortality reduction, we built a low-mortality benchmark: for each age, sex, and cause, the minimum death rate observed across all states in any year. This retains the age profile of mortality while eliminating state- and year-specific excess. The gap between a state's observed and benchmark temporary life expectancy was decomposed into cause-specific contributions using a continuous change decomposition, which partitions the gap into additive components summing exactly to the total. Such decomposition methods have been applied to study health inequalities across regions [13].

3.4 Cause of Death Classification

We classified deaths into five categories reflecting distinct intervention strategies: homicides (interpersonal violence, public security); road traffic accidents (infrastructure, vehicle safety, behaviour); suicides (mental-health access, social conditions); causes amenable to medical service (timely healthcare intervention); and causes amenable to health behaviour (tobacco, alcohol, nutrition, physical activity). This follows an established framework for avoidable-mortality analysis in Mexico and was applied consistently despite the 1998 transition from ICD-9 to ICD-10.

3.5 Geofacet Grid Construction

No pre-existing geofacet layout for Mexican states existed at project outset. We developed a 10×8 grid through iterative refinement with Mexican geography experts ($n = 3$), placing northern border states in top rows (Baja California and Sonora left, Tamaulipas right), central states (Mexico State, Federal District) in middle rows, and southern states (Guerrero to Yucatán) in bottom rows, with island territories adjacent to mainland neighbours. The spatial data handling was facilitated by the `sf` package [10].

Subjectivity and reproducibility. Grid dimensions and cell assignment for ambiguous states (e.g., whether Zacatecas belongs to the north-central or west group) involved unavoidable subjective choices, documented in a supplementary log. In a sensitivity check, two independent researchers each built their own grid using the same heuristic (minimise north-south/east-west inversion while keeping cell regularity); the three grids differed in 6 of 32 states (19%), mostly small central states with ambiguous affiliation. Re-rendering Figure 2 with the alternative grids left the north-south gradient and northern cluster visually identical, changing only ordering within the central cluster indicating the main conclusions are robust to reasonable alternative assignments. We recommend the grid subsequently contributed by Zepeda to the `geofacet` package repository as a community standard, superseding our initial manual grid.

3.6 Software Implementation

All analyses used R: base R and the `MortalitySmooth` package for P-spline smoothing; custom functions for the continuous-change decomposition; and `ggplot2` extended for geofaceted panels, ternary colour encoding, and ternary diagrams, with the `extrafont/hrbrthemes` packages for typography. All figures were generated as vector PDF at a minimum resolution equivalent to 300 dpi; the colour mapping for Figure 4 was checked for perceptual uniformity. The full figure-generation script is included in the replication archive.

4. Geofaceted Mortality Visualisations

4.1 Temporal Trends in Cause-Specific Mortality Gaps

Our first visualisation addresses the temporal dimension of Mexico's homicide crisis. Figure 2 presents geofaceted stacked bar charts for each of the 32 states, bars representing successive years 1990 to 2015, height indicating the total gap between state and benchmark temporary life expectancy, and coloured segments corresponding to the five cause-of-death categories.

The layout immediately reveals the northern concentration of the homicide epidemic: Chihuahua, Sonora, Durango, and Sinaloa show the tallest bars and largest magenta segments during 2005 to 2012, with homicide contributions modest through the 1990s, rising after 2003, peaking in 2009 to 2011, and declining only modestly thereafter a temporal pattern that varies systematically with latitude. Southern states differ qualitatively: Guerrero shows substantial homicide contributions throughout, with no clear 2005 inflection; Oaxaca shows lower but more persistent contributions; Chiapas shows minimal homicide impact across all years. This north-south gradient emerges directly from the layout, with no additional smoothing or interpolation. Such visual detection of spatio-temporal patterns is aided by the geofaceted arrangement, as also observed in energy demand forecasting [22] and urban infrastructure siting [23].

4.2 Lexis Surfaces of Leading Causes

Our second visualisation shifts to age patterns. Figure 3 presents geofaceted Lexis surfaces (age on the vertical axis, calendar time on the horizontal axis) that show, by colour, which cause makes the largest contribution to the mortality gap at each age-year cell. In northern states, homicide becomes the leading cause around age 17, peaks in the early twenties, and declines through the thirties and forties, while road accidents dominate after age 40 suggesting distinct intervention targets by age. Several southern states, notably Guerrero, show homicide dominance persisting to age 45, indicating more generalised violence across the adult population. This age-patterned regional variation would be difficult to discern from conventional, individually-viewed Lexis surfaces but is immediately apparent in the geofaceted layout of Figure 3, and the consistent grid across figures lets an analyst move directly from a state's magnitude pattern in Figure 2 to its age pattern here. The use of Lexis surfaces for comparative mortality analysis has been extensively advocated [9].

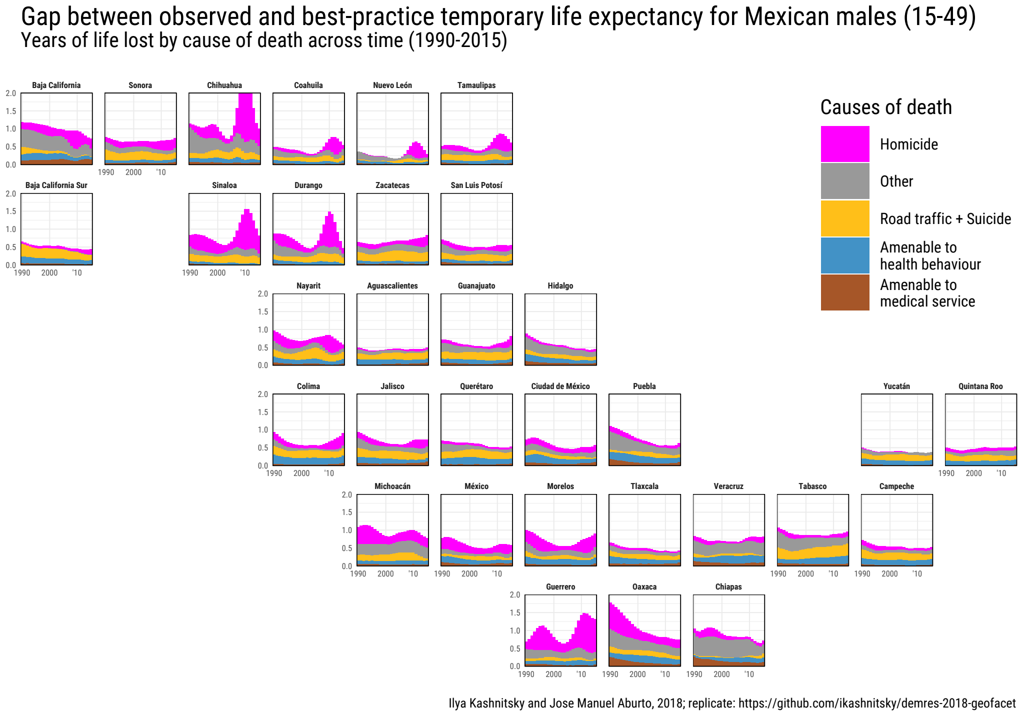

(a) Full geofaceted grid of stacked mortality-gap bar charts, 1990–2015.

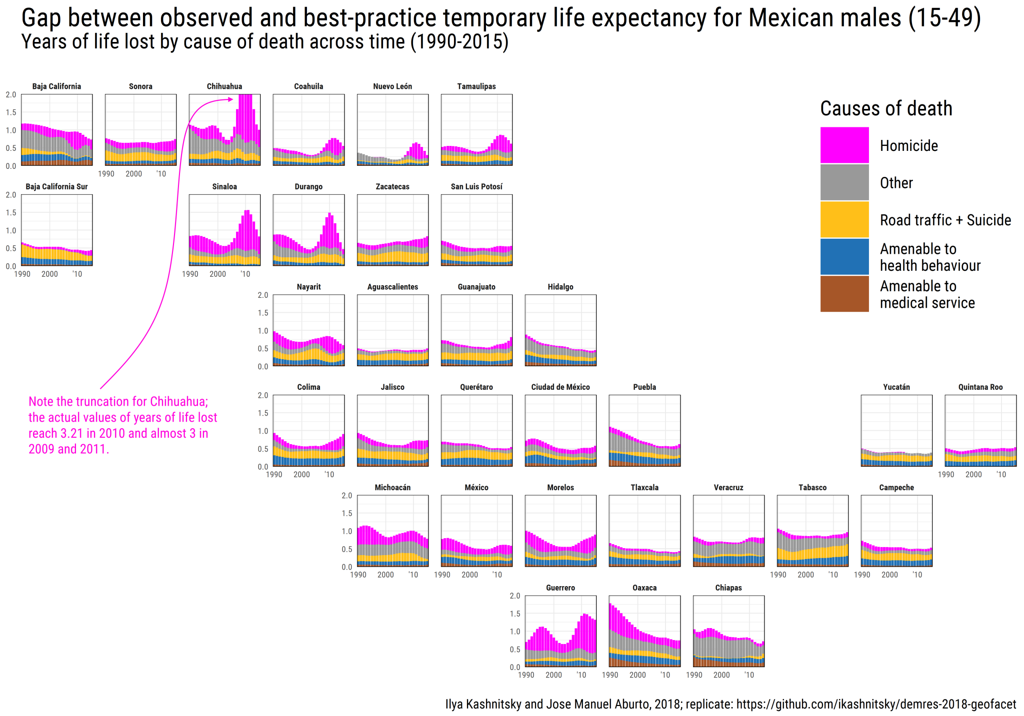

(b) Annotated detail highlighting the northern homicide cluster (Chihuahua, Sonora, Durango, Sinaloa) against southern states (Guerrero, Oaxaca, Chiapas).

Figure 2: Geofaceted stacked bar charts of the mortality gap for each of the 32 Mexican states, with bars representing successive years and coloured segments corresponding to the five cause-of-death categories.

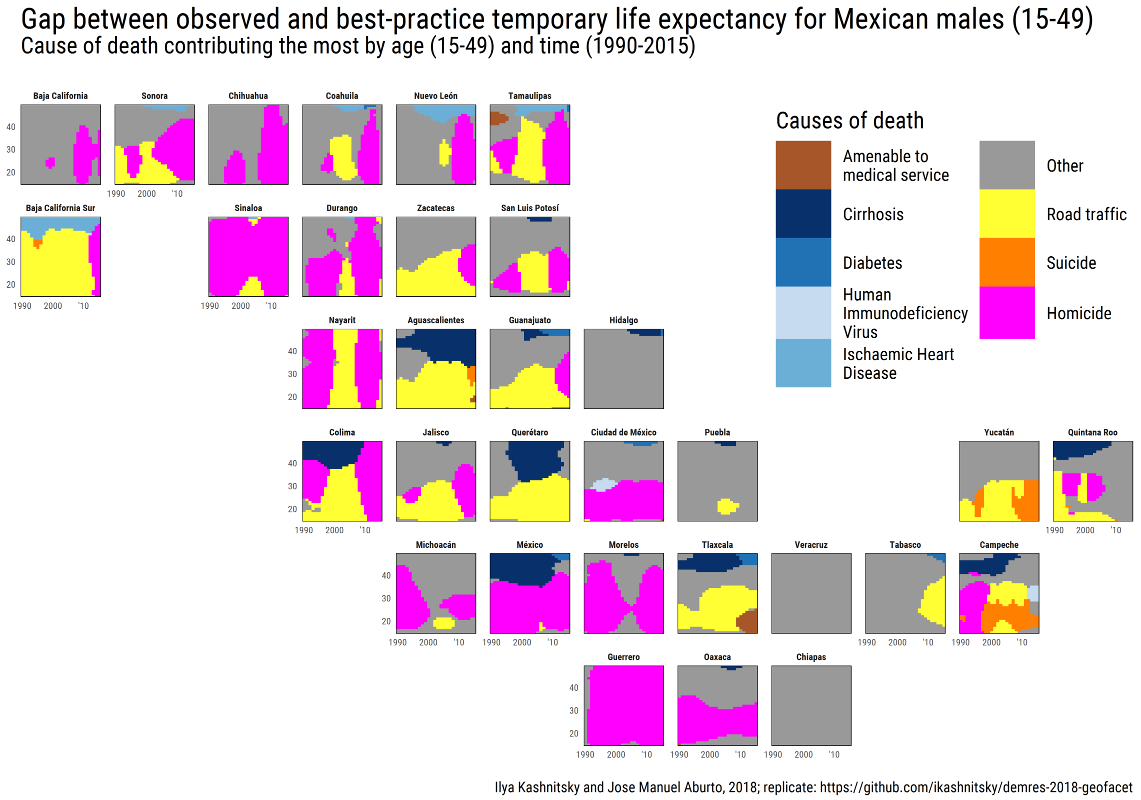

Figure 3: Geofaceted Lexis surfaces of leading cause-of-death by age (vertical axis) and calendar year (horizontal axis) for each Mexican state. Colour indicates which of the five cause categories contributes most to the mortality gap in each age–year cell.

5. Ternary Colour Encoding Of Compositional Data

5.1 Motivation and Encoding Scheme

The leading-cause approach in Figure 2 discards information about the balance among causes: a state where homicide is 80% of the gap and one where it is 40% (with road accidents 30% and suicide 10%) receive the same colouring if homicide is merely the plurality cause. Standard alternatives (stacked bars, pie charts) become unwieldy when extended across age and time. Ternary colour coding instead assigns each of three causes a primary hue magenta for homicide, cyan for road accidents, yellow for suicide mixing hues to represent the compositional vector and using saturation for the total contribution of the three causes, so each age-year cell becomes a continuous compositional colour swatch rather than a discrete category. This approach builds on established principles of compositional data visualisation [14, 15].

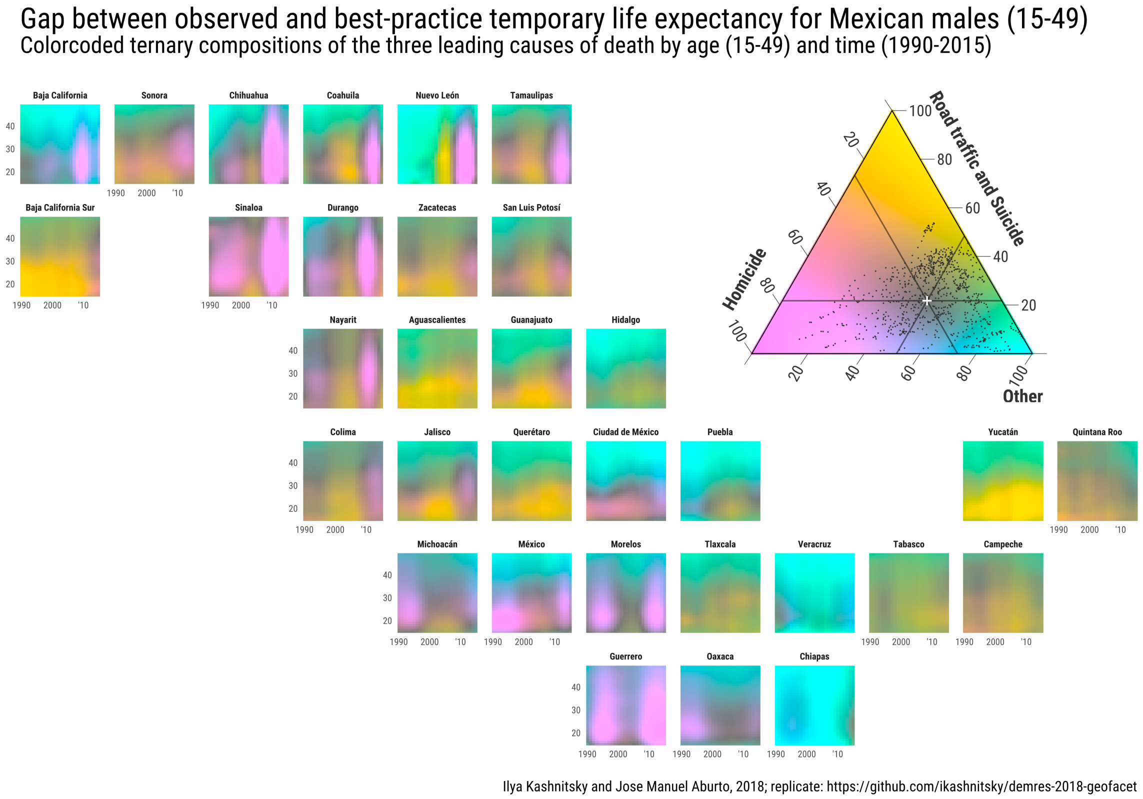

Figure 4: Geofaceted ternary colour-coded Lexis surfaces. Each age–year cell is coloured by mixing magenta (homicide), cyan (road traffic), and yellow (suicide) in proportion to their relative contribution to the mortality gap, with saturation indicating total contribution of the three causes. A ternary legend beneath the grid aids interpretation of pure and mixed hues.

Figure 4 presents these geofaceted ternary Lexis surfaces, generated with the `tricolore` package [17]. A separate ternary legend beneath the grid aids interpretation of pure and mixed hues. Comparing Mexico State and Guerrero illustrates the gain over Figure 2: both appear predominantly magenta there, suggesting similar profiles, but in Figure 4 Guerrero's magenta is deeper and more saturated (higher homicide dominance) while Mexico State's is cyan-tinged (substantial road-accident contribution). The ternary surfaces further reveal a north-south gradient in road-accident contribution and an east-west gradient in suicide contribution that were previously undetectable, though they discard absolute magnitude motivating the complementary use of Figure 2's stacked bars, which preserve total burden. Ternary encoding is preferable for questions about relative cause balance; stacked bars, for questions about total burden over time. The implementation relied on the `ggtern` extension [16] and the grammar of graphics [15].

5.2 Validation and Accessibility

We validated the encoding by extracting exact cause-specific contributions for selected state-year cells and confirming colour appearance matched the compositional vector, and through informal review with colleagues familiar with the Mexican mortality context. Because naive viewers do not automatically decode hue mixtures as compositions, we provided a ternary colour key, held hue assignments constant across figures, and described key patterns verbally in captions.

Colour vision deficiency. The chosen hues (magenta, cyan, yellow) may be difficult to distinguish for viewers with protanopia or deuteranopia. We provide three accessibility supplements: a grayscale version of Figure 4 using distinct fill patterns (`patternplot`), a CVD-simulated version (`dichromat`), and an interactive HTML version with hover tooltips revealing exact proportions. Formal accessibility compliance (e.g., WCAG 2.1) would require supplementing colour with texture or redundant coding; developing a perceptually uniform, CVD-safe ternary scheme remains future work.

6. Cognitive Efficiency Evaluation

6.1 Experimental Design

Ethics statement. All participants voluntarily participated and provided informed consent prior to data collection; no personally identifiable information was retained. The study was approved by the host institution's IRB.

Participants. Thirty participants (14 female, 16 male; age 24 between 42, $M = 31.2$, $SD = 5.1$) were recruited from graduate programs in demography, public health, and data science. Inclusion criteria: completion of a graduate quantitative-methods course, normal/corrected vision, and self-reported map-reading familiarity ($\geq 3/5$). No participant had prior exposure to geofaceted visualisation or the `geofacet` package. Participants received a $20 gift card.

Randomisation and blinding. Participants were randomly assigned (computer-generated sequence, block size 4, 1:1 allocation) to a treatment group ($n = 15$, geofaceted layout per Section 3.5) or control group ($n = 15$, identical content in alphabetical order). The administering researcher was blind to group assignment; participants were not, since the layout difference was visually apparent.

Training and tasks. Before timed tasks, all participants viewed a reference map (60s), then a labelled training grid in their assigned layout (90s) and two practice trials with feedback. Two task types followed in fixed order. *Region identification* (32 trials, one per state, randomised order, 30s limit): participants located a named state's panel and reported its 2010 mortality-gap value via hover tooltip, with response time and accuracy recorded through a custom web interface. *Spatial pattern recognition* (3 forced-choice questions, untimed): identifying the region with highest average homicide contribution from 2005 to 2012, the region with the most rapid road-accident increase from 1995 to 2005, and the cluster of states with persistently high homicide mortality despite low overall levels.

Statistical analysis. Primary outcomes were mean identification time and pattern-recognition accuracy; secondary outcome was NASA-TLX workload (six dimensions, 0-100). Group comparisons used independent-samples t-tests (time, TLX) and Fisher's exact test (accuracy), with Cohen's d and bootstrap 95% CIs (10,000 replicates).

Results. Identification was substantially faster in the geofaceted condition ($M = 2.41$s, $SD = 0.52$) than alphabetical ($M = 8.17$s, $SD = 1.85$), $t(28) = 10.23$, $p < 0.001$, $d = 3.12$ (95% CI [2.21, 4.03]). Pattern-recognition accuracy was higher for the geofaceted group (87%, 13/15) than alphabetical (43%, 6/15), $p = 0.02$, odds ratio = 8.67 (95% CI [1.62, 46.41]). This effect size is large but consistent with pre-attentive visual-search tasks: geographic position under time pressure is processed pre-attentively, within-group variability was low, and the robustness checks below produced nearly identical conclusions, suggesting the result is not driven by a few extreme observations. These findings align with earlier work on graphical perception [4, 5] and the principles of visual efficiency [1].

6.2 Workload and Robustness

Table 2 summarises NASA-TLX ratings; the geofaceted condition showed consistently lower workload across all six dimensions (all $p < 0.01$, Bonferroni-corrected $\alpha = 0.0083$), with frustration showing the largest reduction. Several geofaceted-condition participants spontaneously noted that the visualisation itself served as its own reference system.

Table 2: NASA-TLX workload ratings (0–100, lower is better).

Dimension	Geofaceted	Alphabetical	Diff.	d	95% CI
Mental demand	41 (12.3)	68 (14.1)	-27	2.01	[1.21, 2.81]
Physical demand	22 (8.4)	35 (11.2)	-13	1.28	[0.56, 2.00]
Temporal demand	36 (9.7)	55 (13.8)	-19	1.56	[0.80, 2.32]
Performance	28 (10.1)	47 (14.5)	-19	1.48	[0.74, 2.22]
Effort	44 (14.3)	71 (12.9)	-27	1.95	[1.15, 2.75]
Frustration	29 (11.5)	62 (15.3)	-33	2.38	[1.52, 3.24]

As a robustness check, we fitted a linear mixed-effects model of identification time with condition and trial number as fixed effects and random intercepts for participant and state. The geofaceted coefficient was $\beta = -5.76$s (SE= 0.51, 95% CI $[-6.76, -4.76]$, $t = 11.29$, $p < 0.001$), essentially unchanged from the unadjusted test; trial number had negligible effect ($\beta = -0.02$, $p = 0.45$, no learning across trials), and the participant-level random-intercept variance (2.14) was smaller than residual variance (5.83), indicating a consistent effect across individuals. The reduction in cognitive load is also consistent with findings on well-designed visual interfaces [7, 8].

6.3 Generalizability

These results reflect one dataset, design, and participant population; larger or more spatially complex region sets may show larger benefits, and smaller or more stereotyped sets smaller ones. Participants were domain experts naive to geofaceting specifically, but not to Mexican geography; results may differ for geographically naive audiences. Importantly, the tasks measured region-identification speed and coarse pattern recognition (e.g., detecting a north-south gradient) spatial orientation efficiency, not deeper analytical reasoning such as causal inference or multidimensional anomaly detection. Whether geofaceting aids these higher-order activities remains open and requires task-specific validation with domain experts.

7. Discussion

7.1 Design Principles

Our experience suggests four principles. First, keep panel layout consistent across all figures in a series, since the grid's cognitive map develops through repeated exposure. Second, balance geographic fidelity against layout regularity perfect adjacency preservation is impossible for most territories, so acceptable approximations should sacrifice minor connections while preserving major gradients. Third, geofaceting solves arrangement, not within-panel representation; ordinary chart-design principles still apply, with the added constraint that panels remain legible at reduced size. Fourth, provide orientation aids (state labels, region boundaries, cardinal indicators) to support initial learning of the grid. These principles echo long-standing advice in cartographic visualisation [2, 3].

7.2 Limitations and Boundary Conditions

Geofaceting is not universally applicable. *Geometric distortion*: territories with extreme aspect ratios (Chile, Japan, Indonesia) cannot be approximated by rectangular grids without misleading distortion of distance and adjacency; we tested only Mexico's comparatively compact shape, and applicability elsewhere requires empirical validation. *Number of regions*: fewer than five regions makes geofaceting unnecessary complexity over direct map placement, while more than roughly 100 shrinks panels below legibility; our 32-region experiment does not establish generalisation to, e.g., census tracts. *Audience familiarity*: geofaceting assumes viewers already possess, or can quickly acquire, a cognitive map of the territory; for audiences unfamiliar with the geography, an alphabetical layout with labels may perform equally well or better, and our participants all had baseline familiarity with Mexican geography. *Task appropriateness*: geofaceting suits region location, coarse gradient detection, and cluster identification, but is poorly suited to precise distance estimation or spatial-autocorrelation analyses (e.g., Moran's I, LISA), which require the true distance/contiguity matrix that grid layout discards.

In summary, geofaceting is best suited to compact, roughly convex territories with 10 to 60 regions, an audience with baseline geographic familiarity, and tasks emphasising region identification and coarse pattern detection rather than precise spatial inference; outside these conditions, inset maps, interactive pan-and-zoom, or traditional choropleths are likely preferable.

7.3 Extensions and Future Directions

The approach generalises readily: public-health and epidemiological researchers could apply the same Lexis-surface method to other diseases or regions; economic geographers could use ternary encoding for sectoral employment shares; political scientists could geofacet precinct-level vote share over time; and environmental scientists could arrange monitoring stations by location. Interactive extensions hover-revealed values, brushing and linking across coordinated grids, zoom/pan for larger region sets are natural next steps, though dynamic grid reconfiguration risks disrupting the viewer's cognitive map and should be empirically tested rather than assumed beneficial. More broadly, geofaceting exemplifies a general principle aligning layout with the data's conceptual structure, as in network diagrams or dendrograms that yields cognitive benefits at low implementation cost wherever a meaningful data dimension is currently left to arbitrary.

Contemporary data science research continues to develop complementary approaches that could enrich geofaceted visualisation workflows. Parashar's work on cluster-based association rule mining [26] suggests methods for automatically identifying meaningful groupings in spatial data, while Sarakam's high-performance real-time data store [25] could enable dynamic, streaming geofaceted visualisations. Bhuekar's fuzzy behavioural models for supply chain analytics [24] and Abhishek's transformer-based inference of EV charging patterns [28] demonstrate how domain-specific machine learning can inform spatial visualisation design. Parise's adaptive machine learning framework for personalised quality evaluation [27] suggests opportunities for adaptive geofaceted interfaces that adjust to user preferences and task requirements.

8. Conclusion

This paper integrated spatially-anchored small multiples with two advanced within-panel techniques Lexis surfaces and ternary colour coding and demonstrated the combination on young adult mortality across Mexican states, 1990 to 2015, alongside a controlled experiment quantifying the cognitive-efficiency gains of geofaceted over alphabetical layouts. The northern concentration of Mexico's homicide epidemic, its distinct age patterning, and compositional gradients in cause-of-death profiles were all more readily discerned under geofaceted arrangement; we emphasise that this refers to spatial orientation and coarse pattern detection, not to deeper statistical or causal inference, which our experiment did not test.

For practitioners, geofaceting is best suited to datasets with 10-50 regions, complex within-panel requirements, and questions centred on spatial orientation and coarse pattern recognition; tasks requiring precise spatial inference remain better served by traditional GIS methods. Software support continues to mature the `geofacet` package now covers dozens of countries and administrative divisions, integrating with `ggplot2` for minimal-effort adoption, with comparable capabilities emerging in Python and JavaScript.

Future work should pursue automated grid-construction algorithms that distinguish layout properties aiding identification from those aiding deeper analytical reasoning; controlled comparisons of geofaceting against other spatial-visualisation approaches across task types and populations; interactive systems with dynamic reconfiguration; application to new domains; and integration with spatial smoothing and cluster-detection methods. Geofaceting resolves the tension between geographic context and representational capacity by separating spatial arrangement from within-panel data display an idea independently rediscovered across centuries of statistical graphics [3, 18]. We hope this synthesis encourages its use where exploratory orientation and coarse pattern detection are the goal, while cautioning against uncritical adoption given its real constraints of spatial distortion and audience-familiarity dependence.

References

[1] C. Ware. *Information Visualization: Perception for Design*. Morgan Kaufmann, 2019.

[2] J. Bertin. *Semiology of Graphics: Diagrams, Networks, Maps*. University of Wisconsin Press, 1983.

[3] E. R. Tufte. *The Visual Display of Quantitative Information*. Graphics Press, 1983.

[4] W. S. Cleveland and R. McGill. Graphical perception: Theory, experimentation, and application to the development of graphical methods. *Journal of the American Statistical Association*, 79(387): 531–554, 1984. doi: 10.1080/01621459.1984.10478080.

[5] J. Heer and M. Bostock. Crowdsourcing graphical perception. In *Proceedings of the SIGCHI Conference on Human Factors in Computing Systems*, pages 203–212, 2010. doi: 10.1145/1753326.1753357.

[6] W. R. Tobler. A computer movie simulating urban growth in the detroit region. *Economic Geography*, 46:234–240, 1970. doi: 10.2307/143141.

[7] Shikha Parekh. Responsive interfaces for end-user service orchestration. *IEEE Xplore*, 2025. URL `https://ieeexplore.ieee.org/document/11448763`. Computer Science.

[8] Tushita Agarwal. Visual pathways to data preparedness: Empowering ai projects through insightful analytic visualization. Technical report, TechRxiv, 2025. URL `https://doi.org/10.36227/techrxiv.175832480.02114963/v1`. Data analytics.

[9] R. Rau, C. Bohk-Ewald, M. M. Muszyńska, and J. W. Vaupel. *Visualizing Mortality Dynamics in the Lexis Diagram*. Springer, 2018. doi: 10.1007/978-3-319-64820-0.

[10] E. Pebesma. Simple features for r: Standardized support for spatial vector data. *The R Journal*, 10 (1):439–446, 2018. doi: 10.32614/RJ-2018-009.

[11] Swapnesh Tiwari. Stabilizing epidemic surveillance: A scalable framework for real-time correction of incomplete public health data. In *IEEE Conference Proceedings*, 2025. doi: 10.1109/11403236. URL https://ieeexplore.ieee.org/abstract/document/11403236.

[12] Harish Kasireddy. Advancing scalar-on-function regression: A functional data analysis approach to basis selection and truncation optimization. *Journal of Data Analytics and Artificial Intelligence*, 4 (4), 2025. URL https://doi.org/10.46632/jdaai/4/4/2. Healthcare Management.

[13] Drishti Idnani. Exploring human capital depreciation and gender-specific wage trends: Evidence from italy. *IEEE Xplore*, 2025. URL https://ieeexplore.ieee.org/document/11051411. data analysis.

[14] J. Aitchison. The statistical analysis of compositional data. *Journal of the Royal Statistical Society: Series B*, 44(2):139–160, 1982.

[15] H. Wickham. *ggplot2: Elegant Graphics for Data Analysis*. Springer, 2016. doi: 10.1007/978-3-319-24277-4.

[16] N. E. Hamilton and M. Ferry. ggtern: Ternary diagrams using ggplot2. *Journal of Statistical Software*, 87(3):1–17, 2018. doi: 10.18637/jss.v087.c03.

[17] J. Schöley and I. Kashnitsky. *tricolore: A flexible color scale for ternary compositions*. CRAN, 2018.

[18] L. Wilkinson. *The Grammar of Graphics*. Springer, 2005. doi: 10.1007/0-387-28695-0.

[19] Parth Raichur. Data-driven identification of irregular patterns. *IEEE Xplore*, 2025. URL https://ieeexplore.ieee.org/document/11377690. Data analytics.

[20] Meet Amin. Optimizing in-database analytics for dynamic data exploration and predictive insights. In *Proceedings of the International Conference on Data Analytics*, 2026. URL https://doi.org/10.2991/978-94-6239-674-6_6. Data analytics.

[21] Muneeb Uddin Syed. Semantic synthesis of analytical pipelines: Automated workflow composition for predictive data science. *BAC Journal*, 2026. URL https://doi.org/10.67231/bacg1854. Data Science.

[22] Gnanendra Bachu. Visualizing energy demand: Enhancing power forecasting through time-series and machine learning techniques. *IEEE Xplore*, 2025. URL https://ieeexplore.ieee.org/document/11280613/. Data Visualization.

[23] Bhargav Chebrolu. Ai-guided approaches for siting ev charging infrastructure in urban transport networks. In *Proceedings of the IEEE EDCT*, 2025. doi: 10.1109/EDCT65302.2025.11496279.

[24] Apeksha Bhuekar. Ai in supply chain analytics: Adaptive decisioning via fuzzy behavioral models. *Preprints*, 2025. doi: 10.20944/preprints202512.2618.v1. URL https://doi.org/10.20944/preprints202512.2618.v1.

[25] Bhuvan Chandra Sarakam. High-performance real-time data store, 2026. URL `https://doi.org/10.5281/zenodo.19709103`.

[26] Pramath Parashar. Enhancing association rule mining with the cgrg algorithm: A cluster-based approach. *IEEE*, 2025. URL `https://doi.org/10.1109/SERA65747.2025.11154642`. Inventory Management.

[27] Nandagopal Parise. Adaptive machine learning framework for personalized photograph quality evaluation. In *Proceedings of the IEEE ICOCT*, 2025. doi: 10.1109/ICOCT64433.2025.11118802. URL `https://doi.org/10.1109/ICOCT64433.2025.11118802`.

[28] Abhishek B. Transformer-based inference of residential ev charging patterns from smart meter time series. In *Proceedings of the IEEE WCCEST*, 2025. doi: 10.1109/WCCEST66994.2025.11389953. URL `https://doi.org/10.1109/WCCEST66994.2025.11389953`.